Structure and mechanism of activity-based inhibition of the EGF-Receptor by Mig6

Eunyoung Park[#1,2], **Nayoung Kim**[#3,4], **Scott B. Ficarro**[1,5], **Yi Zhang**[1,5], **Byung Il Lee**[1,6], **Ahye Cho**[3,4], **Kihong Kim**[4], **Angela K.J. Park**[3,4], **Woong-Yang Park**[3,4], **Bradley Murray**[7], **Matthew Meyerson**[7,8,9], **Rameen Beroukhim**[1,7,8,10], **Jarrod A. Marto**[1,2,5], **Jeonghee Cho**[3,4], and **Michael J. Eck**[1,2]

[1]Department of Cancer Biology, Dana-Farber Cancer Institute, Boston, MA USA

[2]Department of Biological Chemistry and Molecular Pharmacology, Harvard Medical School, Boston, MA USA

[3]Samsung Genome Institute, Samsung Medical Center, Seoul, Republic of Korea

[4]Samsung Advanced Institute for Health Sciences and Technology, SungKyunKwan University, Seoul, Republic of Korea

[5]Blais Proteomics Center, Dana-Farber Cancer Institute, Boston, MA USA

[6]Biomolecular Function Research Branch, Division of Convergence Technology, Research Institute, National Cancer Center, Goyang, Gyeonggi Republic of Korea

[7]Broad Institute of Harvard and MIT, Cambridge, MA USA

[8]Department of Medical Oncology, Dana-Farber Cancer Institute, Boston, MA USA

[9]Department of Pathology, Harvard Medical School, Boston, MA USA

[10]Department of Medicine, Harvard Medical School, Boston, MA USA

[#] These authors contributed equally to this work.

Abstract

Mig6 is a feedback inhibitor that directly binds, inhibits and drives internalization of ErbB-family receptors. Mig6 selectivity targets activated receptors. Here we find that the EGF receptor phosphorylates Mig6 on Tyr394, and that this phosphorylation is primed by prior phosphorylation of an adjacent residue, Tyr395, by Src. Crystal structures of human EGFR–Mig6 complexes reveal

the structural basis for enhanced phosphorylation of primed Mig6 and show how Mig6 rearranges after phosphorylation by EGFR to effectively irreversibly inhibit the same receptor that catalyzed its phosphorylation. This dual phosphorylation site allows Mig6 to inactivate EGFR in a manner that requires activation of the target receptor and can be modulated by Src. Loss of Mig6 is a driving event in human cancer; analysis of 1057 gliomas reveals frequent focal deletions of *ERRFI*, the gene that encodes Mig6, in EGFR-amplified glioblastomas.

Introduction

The cytosolic protein Mig6 (the product of mitogen inducible gene 6, now formally designated *ERRFI1*) is a feedback inhibitor of the epidermal growth factor receptor (EGFR) and other ErbB family members[1–4]. Mig6 expression is induced by EGFR signaling via the Ras Map kinase pathway[5], as well as by other mitogenic and stress stimuli[6]. Mig6 directly binds to EGFR and inhibits its signaling both by inhibiting the catalytic activity of the kinase[7–9] and by directing its internalization and degradation[10,11]. Deletion of the Mig6 gene in the mouse hyperactivates EGFR signaling, leading to skin hyperplasia and spontaneous tumor formation in skin, lung and other tissues[12,13]. A recent study showed that loss of Mig6 promotes tumor initiation and progression in a mouse model of mutant EGFR-driven lung adenocarcinoma[14]. In humans, Mig6 expression is diminished in a number of tumors[12,15], and the *ERFFI1* chromosomal locus (1p36) is a frequent site of deletion in multiple tumor types[6].

The domain structure of Mig6 includes an N-terminal CRIB domain, a motif that mediates association with the Rho-family GTPase Cdc42[16], and a more C-terminal ErbB-binding region that is necessary and sufficient for binding and inhibition of EGFR[7,8,17]. Functional dissection of this region has identified a fragment that binds EGFR (Mig6 residues 336–364, termed segment 1), but lacks full inhibitory activity[8,18]. Inclusion of ~50 additional residues (segment 2, residues 365–412) is required for potent inhibition of EGFR in vitro and in cells. Based in part on a crystal structure of Mig6 segment 1 in complex with EGFR, Mig6 was proposed to inhibit EGFR in an allosteric manner by blocking formation of the activating receptor dimer[8]. No structural information is available for Mig6 segment 2, and how it contributes to inhibition is not understood at a mechanistic level. Furthermore, a particularly interesting and crucial aspect of Mig6 function – its ability to specifically target the activated form of the receptor – remains unexplained[1,2,17].

EGFR is a key regulator of cellular proliferation, migration and survival and is among the most frequently altered proteins in human cancer, in particular glioblastoma and lung adenocarcinoma[19–22]. In non-small cell lung cancer, common oncogenic alterations in the EGFR kinase domain include the L858R point mutation, deletions within exon 19 (Ex19Del), and insertions in the region encoded by exon 20 (Ex20Ins)[23]. Lung cancer patients whose tumors are driven by certain of these mutations respond well to EGFR kinase inhibitors including gefitinib, erlotinib and afatinib[24,25], but secondary resistance mechanisms limit their long term efficacy[26]. Genomic alterations in the extracellular, carboxy-terminal and catalytic regions of EGFR have been identified in glioblastoma and

EGFR amplifications are a hallmark of the classic subtype of this disease[21,27–30]. However, EGFR inhibitors have not yielded dramatic responses in glioblastoma patients to date.

A recent investigation of the substrate specificity of EGFR using an in vitro peptide-library approach revealed that it preferentially phosphorylates substrates that are already phosphorylated on a tyrosine residue in the P+1 position (M.J.E., C. Yun, M. Begley and L. Cantley, unpublished data). Phosphorylation of such "primed" sites will therefore lead to doubly phosphorylated "pYpY" elements in cognate substrates. Interestingly, Mig6 can be phosphorylated on two adjacent tyrosine residues (Y394 and Y395) in an EGFR or ErbB2-dependent manner[14,31,32]. This site lies in the crucial segment 2 region of Mig6, but the functional consequences of phosphorylation on these residues have not been clearly elucidated. Very recently, phosphorylation on Y394 has been reported to diminish the ability of Mig6 to inhibit EGFR[33], and to promote increased binding to the receptor[14].

We set out to elucidate the role of this dual phosphorylation site in Mig6 function at a structural and mechanistic level. We find that Y394-phosphorylated Mig6 directly inhibits EGFR in a peptide substrate-competitive manner. Tyrosine 394 is phosphorylated by EGFR itself, and this phosphorylation underlies the selectivity of Mig6 for activated receptors. Tyr394 phosphorylation is dramatically accelerated by prior phosphorylation of Y395, a site that is preferentially phosphorylated by Src. Small molecule inhibition and shRNA-mediated knockdown of Src diminished levels of Mig6 phosphorylation on this site, and Y395F mutant Mig6 is impaired in its ability to inhibit transformation by oncogenic EGFR mutants. Crystal structures explain the priming effect of Y395 phosphorylation and show that once phosphorylated on Y394, segment 2 rearranges to form a hairpin-like element that blocks the peptide-substrate binding cleft. Segment 1 binds the EGFR C-lobe, anchoring segment 2 and rendering it an effective substrate-competitive inhibitor. Collectively, our results indicate that Mig6 is an activity-based inhibitor of EGFR; it exploits the phosphotransfer activity of a target receptor molecule to inactivate it. This negative feedback mechanism is subverted in human tumors; we find that the Mig6 gene *ERRFI1* is frequently deleted in EGFR-amplified gliomablastomas.

Results

Mig6 is phosphorylated on Y394 and Y395 by activated EGFR

Using quantitative tandem mass spectrometry[34], we analyzed the phosphoproteome of NIH-3T3 cells stably expressing WT or oncogenic mutant EGFR (see Supplementary Fig. S1 and Table S1). To complement previous phosphoproteomic studies that focused on the L858R and Ex19Del EGFR mutants[14,31,35], we analyzed an exon20 insertion mutant (insNPG) and an oncogenic C-terminal deletion mutant (CTDel1, which deletes residues 1010-1152)[36–38]. We included a kinase-dead (D837A) version of the exon20 insertion mutant as a negative control. Among more than 500 proteins that we found were hyperphosphorylated in EGFR-mutant cells, we identified a doubly phosphorylated Mig6 pY394pY395 peptide (Fig. 1a).

To further explore the genesis and functional consequences of Mig6 phosphorylation on Y394 and Y395, we raised a phospho-specific antibody against the dual pY394pY395 site

(Supplementary Figs. S2a, b). Immunoblotting with this anti-pMig6 antibody revealed constitutive phosphorylation on this site in NIH-3T3 cells stably expressing mutant EGFR, and EGF-induced phosphorylation in cells expressing WT EGFR (Fig. 1b). In addition, we found that endogenous Mig6 was constitutively phosphorylated in PC9 and HCC827 lung cancer cell lines, which harbor *EGFR* Ex19 deletion mutations (Fig. 1c, lanes 1 and 3). This Mig6 phosphorylation was abolished by treatment with the EGFR inhibitor erlotinib (Fig. 1c, lanes 2 and 4), suggesting that active EGFR is responsible for phosphorylation of Mig6.

EGFR phosphorylates Y394 primed by Y395 phosphorylation

We next examined the ability of EGFR to directly phosphorylate 10-residue synthetic peptides spanning this site (residues 390-399) that were either unphosphorylated (YY) or already phosphorylated on either Y394 or Y395 (designated pYY and YpY, respectively). The purified kinase domains of both WT EGFR and the L858R mutant were able to phosphorylate the YY peptide, but the rate of phosphorylation of the YpY peptide was dramatically faster (Fig. 2a). This priming effect was specific for the P+1 phosphorylation in the YpY sequence, as the rate of phosphorylation of the pYY peptide was similar to that of the unphosphorylated YY species. Using quantitative mass spectrometry, we further studied EGFR phosphorylation of the YY peptide in order to determine whether one or both of tyrosines 394 and 395 is phosphorylated (Fig. 2b). The major product of the reaction was pYY, the Y394-phosphorylated species, but the YpY and pYpY species were also produced at lower levels. We also observed preferential phosphorylation of Y394 by EGFR when a longer Mig6 fragment encompassing both segment 1 and 2 was used as substrate (residues 330-399, Supplementary Figs. S2c, d).

Although EGFR can phosphorylate Y394 absent prior phosphorylation on Y395, the results above suggest that phosphorylation of Y394 could be primed by prior phosphorylation of Y395 by a different kinase. Src-family kinases are an obvious candidate for this role, as Src is activated in the course of EGF signaling. Thus we examined the same 10-residue Mig6 YY peptide as a substrate for c-Src. In contrast to EGFR, the major product of Src phosphorylation was YpY, the Tyr395-phosphorylated species (Fig. 2c). We conclude that EGFR preferentially phosphorylates Mig6 on Tyr394, and that this phosphorylation is markedly accelerated by prior phosphorylation of Tyr395. Src preferentially phosphorylates Y395, and is a candidate kinase for this priming phosphorylation.

EGFR inhibition requires the Y394 site and is modulated by Src

Tyrosines 394 and 395 and surrounding residues are highly conserved in both Mig6 and Ack1, a non-receptor tyrosine kinase that shares a large region of homology with Mig6[39,40]. Thus we sought to understand the functional effect of their phosphorylation. Expression of ligand-activated WT or oncogenic mutant EGFR transforms NIH-3T3 cells, but transformation is completely blocked by co-expression of WT Mig6, as assessed by soft agar colony formation (Figs. 3a–c). By contrast, Y394F and Y394F Y395F mutant Mig6 proteins were markedly impaired in their ability to inhibit EGFR-driven transformation (Figs. 3a–c). The Y395F mutant was also modestly impaired. Wild type Mig6 effectively blocked EGF-induced phosphorylation of the WT receptor in these cells, but Y394F Y395F mutant Mig6 did not (Fig. 3d). A similar effect was apparent in cells expressing mutant

EGFR (Supplementary Figs. S3a, b). Further, we probed binding of Mig6 to EGFR in co-immunoprecipitation experiments with cell lysates prepared from HEK-293T cells co-expressing WT or mutant Mig6 with L858R EGFR. While WT Mig6 was found in complex with L858R EGFR (Fig. 3e, lane 1), co-precipitation of Mig6 with L858R EGFR was markedly diminished by mutation of these phosphorylation sites (Fig. 3e, lanes 2 and 4) and by erlotinib (Supplementary Fig. S3c). Taken together, these results indicate that the Y394–Y395 phosphorylation site in Mig6 is critical for its ability to effectively bind and inhibit both WT and mutant EGFR, and to block cellular transformation driven by activated EGFR.

We examined the role of c-Src in Mig6 phosphorylation and subsequent binding and inhibition of EGFR using both pharmacologic and shRNA approaches to silence c-Src activity. Treatment of NIH-3T3 cells stably coexpressing WT EGFR and Mig6 with the Src inhibitor dasatinib attenuated EGF-induced phosphorylation of Mig6 on Y394–Y395 (Figs. 3f, g). Dasatinib treatment also decreased co-immunoprecipitation of EGFR with Mig6 (Fig. 3f). At 0.5 μM, dasatinib effectively blocked c-Src activation-loop autophosphorylation (on Y416) and decreased Mig6 phosphorylation in a dose-dependent manner (Fig. 3f, lane 8). We also noted increased EGF-induced phosphorylation of EGFR at increasing concentrations of dasatinib (Fig. 3f, lanes 2, 4, 6 and 8), consistent with diminished Mig6-mediated receptor inhibition. Src also modulated Mig6 phosphorylation and function in lung cancer cell lines PC9 and A549, which are driven by mutations in *EGFR* and *KRAS*, respectively. We generated PC9 and A549 cells with stable knockdown of c-Src kinase by expressing shRNA targeting c-Src via lentiviral infection, and found that EGF-induced phosphorylation of Mig6 on Y394–Y395 was reduced in PC9 cells and not detected in A549 cells following Src knockdown (Fig. 3h).

Y394 phosphorylation underlies activity-based EGFR inhibition

We tested the ability of a segment 1+2 fragment of Mig6, either WT (Mig6-YY) or with phenylalanine substitutions in Tyr394 and Tyr395 (Mig6-FY, YF and FF) to inhibit purified EGFR kinase. While the Mig6-YY and Mig6-YF mutant proteins potently inhibited the kinase, the FY and FF mutants had little activity (Fig. 4a). To specifically determine if phosphorylation of these residues is required for EGFR inhibition, we prepared semi-synthetic Mig6 segment 1+2 proteins in defined phosphorylation states using intein-mediated expressed protein ligation[41] (Supplementary Figs. S4a, b) and examined the time course of their inhibition of EGFR. All four Mig6 phosphorylation variants were similar in their potency at steady-state (YY, pYY, YpY, and pYpY, Supplementary Figs. S4c, d), and they also potently inhibited the intact, ligand-bound EGF receptor (Supplementary Fig. S4e). However, inhibition of EGFR kinase by the YY variant was strongly time-dependent (Figs. 4b, c). Its potency increased by two orders of magnitude during the course of the reaction with WT EGFR, from ~1 μM at the initial time point to 10–20 nM after 20 minutes. By contrast, Mig6-pYY and Mig6-pYpY exhibited 10–20 nM potency from the earliest time points. We observed a modest but reproducible time-dependent increase in the potency of the Mig6-YpY protein, and a more rapid plateau (~12.5 min), consistent with more rapid phosphorylation of Y394 when Y395 is already phosphorylated. These findings clearly indicate that Mig6 requires phosphorylation on Y394 in order to inhibit EGFR; i.e. that Mig6-pYY and Mig6-pYpY are the actual inhibitory species.

To directly examine whether phosphorylation of Y394 is associated with EGFR binding and inhibition, we combined the EGFR kinase domain with an approximate 2-fold excess of Mig6-YY under reaction conditions for 20 minutes, and separated the products by size-exclusion chromatography (Fig. 4d). Strikingly, all of the Mig6 that co-eluted with EGFR was phosphorylated, as judged by a shift in electrophoretic mobility of the phosphorylated species and by western blotting with the Mig6 phospho-specific antibody, whereas little if any of the free Mig6 was phosphorylated.

The lack of phosphorylation of excess Mig6 in this experiment suggested that Mig6 might function as an "activity-based" inhibitor of EGFR; i.e. that once phosphorylated on Y394, it could remain bound to inhibit the same EGFR molecule that catalyzed its phosphorylation. This is a defining property of small molecule "mechanism-based" inhibitors, which are exquisitely selectivity for their intended target because no free pool of active inhibitor is created[42]. To test this notion, we co-expressed active Myc-tagged EGFR (L858R) and kinase-dead HA-tagged EGFR (L858R/D837N) along with WT Mig6 in HEK-293T cells, and examined the levels of Mig6 bound to either the L858R or L858R/D837N mutant by co-immunoprecipitation. Levels of expression of the two EGFR mutants were similar, but virtually all of the Mig6 co-precipitated with the catalytically active L858R EGFR (Fig. 4e), despite the fact that the kinase-dead mutant retains the ability to bind phosphorylated Mig6 (Supplementary Fig. S5a). Measurement of the rate of dissociation of phosphorylated Mig6 from EGFR in vitro revealed a half-life of ~45 min for the complex (Supplementary Fig. S5b), which is long in comparison with the 5–10 minutes required for internalization of activated EGFR in cells[10,43]. We conclude that Mig6 requires phosphorylation on Y394 for potent inhibition of EGFR. EGFR carries out this phosphorylation, and the rate of dissociation of phosphorylated Mig6 is sufficiently slow that it allows Mig6 to function as an activity-based inhibitor of the receptor.

Structural snapshots of Mig6 inhibition of EGFR

To see how Mig6 inhibits EGFR, we determined three crystal structures of Mig6 fragments bound to EGFR, representing distinct steps in the course of Mig6 inhibition (Table 1 and Fig. 5). Structures of the kinase in complex with 10-residue Mig6-YpY and Mig6-pYpY peptides explain the priming effect of Y395 phosphorylation (Fig. 5a, b). In the Mig6-YpY structure, the kinase adopts an active conformation and the Mig6 peptide interacts with the activation loop in an anti-parallel manner as seen in other kinases in complex with peptide substrates[44]. Y394 is in the phospho-acceptor position, and the backbone amide and carbonyl groups of pY395 (in the P+1 position) hydrogen bond with the backbone groups of Val876 in the EGFR activation loop (Fig. 5d). The sidechain of pY395 extends across Ala920 and its phosphate group is positioned to hydrogen bond with Lys879 and with the backbone amide of Ala920. These interactions in the P+1 "priming pocket" explain the enhanced phosphorylation of the pY395-phosphorylated Mig6 peptide.

Interestingly, we observed a closely similar mode of binding with the doubly-phosphorylated Mig6-pYpY peptide (Fig. 5b, e). The sidechain of pY394 is positioned in the phosphoacceptor site, despite the fact that it is phosphorylated (Supplementary Fig. S6a), and pY395 is again observed in the P+1 priming pocket. As explained below, the structure

of a longer fragment of phospho-Mig6 bound to EGFR reveals that segment 2 rearranges after phosphorylation of Y394, leading us to conclude that this Mig6-pYpY peptide complex represents a transient intermediate in phosphorylation-dependent inhibition.

The structure of the complete, doubly-phosphorylated EGFR-binding region of Mig6 (residues 330-399) in complex with EGFR reveals that segment 1 binds across the base of the C-lobe as previously described[8], while segment 2 forms a β hairpin-like element that occupies the peptide-substrate binding site (Fig. 5c). Phosphorylated tyrosines 394 and 395 occupy the peptide-substrate site, but the register of the polypeptide chain shifts by one residue as compared with the structures above such that pY394 occupies the P+1 priming position and histidine 393 occupies the phosphoacceptor pocket (Fig. 5f). Likewise, pY395 shifts into the P+2 position. The more N-terminal portion of segment 2 folds back to hydrogen bond with the pY394–pY395 region to create the β hairpin-like structure. The phosphate groups of both phosphotyrosine residues make favorable electrostatic interactions; pY395 with lysine 875 in EGFR and pY394 with lysine 879 in EGFR (Fig. 5f, Supplementary Fig. S6b).

Consistent with the structure, kinetic studies confirm that Mig6 inhibits EGFR in a peptide substrate competitive manner with a Ki=15.85 nM (Supplementary Fig. S7a, b). A V948R substitution in the Mig6 segment 1 binding site on EGFR decreases the potency of inhibition in vitro by Mig6 segment 1 + 2 (Supplementary Fig. S7c), thus interactions of segment 1 are also important for potent inhibition. We propose that segment 1 effectively anchors segment 2 to the kinase, rendering it an effective substrate-competitive inhibitor once it is phosphorylated.

ERRFI1 is focally deleted in EGFR-amplified glioblastoma

The Mig6 gene *ERRFI* was previously noted as one of two genes in a minimal common region of deletion across 18 glioblastoma tumors and 20 cell lines[11]. To better understand the significance of Mig6 loss in glioblastoma and lower-grade gliomas, we analyzed 1057 gliomas characterized by The Cancer Genome Atlas (TCGA) project[21]. *ERRFI1*, which resides on chromosome 1p36, is in the third most significantly deleted region across all 1057 tumors, following deletions of the well-known tumor suppressors *CDKN2A/B* and *PTEN* (Figs. 6a, b). In a separate analysis of the 571 glioblastomas in this dataset, *ERRFI1* is the only gene in the "peak region" where deletions in different samples overlap most frequently (Fig. 6c). Deletions of *ERRFI1* are primarily hemizygous and are present in 24% of glioblastomas, of which 21% are focal events that encompass less than half of chromosome 1p. *ERRFI1* is also deleted in 42% of 486 lower-grade gliomas characterized by TCGA, but of these 37% are large deletions that encompass most of chromosome 1p and occur primarily in oligodendrogliomas with mutations of *FUBP1*, a known tumor suppressor in these gliomas that resides on 1p31 (ref. 45). Interestingly, *ERRFI1* deletions were highly correlated with co-existing focal amplifications of *EGFR*. Across all 1057 TCGA gliomas in our analysis, 27% of tumors with focal amplification of *EGFR* also exhibited focal deletions of *ERRFI1*, as compared to 8% of the tumors without *EGFR* amplification (Fig. 6c). This is a significant association (p=0.00014), even after controlling for lineage and for variations in overall levels of genomic disruption in these samples[46].

Discussion

Our studies reveal a heretofore-unappreciated mechanism of specificity in Mig6-mediated inhibition; the Mig6 protein is impotent until phosphorylated on Y394 by EGFR itself, and once phosphorylated Mig6 remains bound to inhibit the receptor that catalyzed its phosphorylation, likely until internalization and degradation of the receptor (Fig. 7a). This mechanism allows Mig6 to selectively target active receptor molecules. To our knowledge, activity-based inhibition has not been previously described as part of an endogenous regulatory circuit. The bipartite structure of the Mig6 inhibitory element is well-suited to this purpose. The Y394–Y395 phosphorylation site in segment 2 detects active EGFR molecules and rearranges to directly inhibit the kinase by occupying the peptide substrate-binding site. This rearrangement presumably requires local dissociation of segment 2, but binding of segment 1 is structurally independent of segment 2, allowing it to anchor Mig6 to an active receptor in the course of phosphorylation and subsequent rearrangement into the high-affinity complex we observe here. Phosphorylation of the Y394–Y395 site will also stabilize the interaction of segment 1 with the kinase C-lobe, preventing a Mig6-bound receiver subunit from subsequently acting in an activator role, because it blocks the asymmetric dimer interface[8]. While we have not explicitly examined the effect of Y394 phosphorylation on EGFR internalization and degradation, we reason that it must also control these events because they require stable association of Mig6 with the active receptor.

In conflict with our findings, a prior biochemical study found that Y394 phosphorylation diminishes the ability of Mig6 to inhibit EGFR[33]. This conclusion was based on an experiment using semisynthetic Mig6-pY394 to inhibit nearly full-length ligand-bound EGFR (tEGFR). The discrepancy is unlikely a result of differences in EGFR constructs or kinase assays employed, as our phosphorylated Mig6 segment 1+2 preparations potently inhibited tEGFR under conditions used in the earlier study (Supplementary Fig. S4e). The Mig6 construct employed in the earlier study introduced three substitutions near pY394 (S390P, S391G, and T392C). In particular, mutation of Thr392 may have affected EGFR inhibition as this residue contacts the kinase and also hydrogen bonds with His393, the Mig6 residue that occupies the phosphoacceptor site in the inhibited complex (Fig. 5f).

We further found that Mig6 inhibition of EGFR is modulated by Src via phosphorylation of Mig6 on Y395. Prior phosphorylation of Y395 dramatically increases the rate of EGFR phosphorylation of Mig6 on Y394 in vitro, and suppression of Src activity pharmacologically or by shRNA decreased phosphorylation of Mig6 on this site in cells, impairing EGFR binding and inhibition. We do not observe a marked difference in the potency of inhibition of EGFR by the doubly phosphorylated site as compared with the singly Y394-phosphorylated species, thus the role of priming by Src may be limited to its effect on EGFR-mediated phosphorylation of Y394. Priming may serve to accelerate the time course and/or efficiency of Mig6 inhibition of EGFR when Src is also active. We do not exclude the possibility that other kinases in addition to Src could also contribute to priming. One candidate is c-Abl, which can bind to Mig6 and phosphorylate the Y394–Y395 site[47].

Deletions involving the 1p36 locus have been noted in a wide variety of human malignancies, prompting efforts to identify one or more tumor suppressive genes in this region[48]. Our analysis points to *ERRFI1* as the most significantly deleted 1p gene in the gliomas we studied. We found focal deletions of *ERRFI1* in approximately one-fifth of the glioblastomas analyzed. *ERRFI1* loss was most often hemizygous. Because Mig6 inhibits EGFR on a strict per-molecule basis, reduced *ERRFI1* gene dosage and consequent lower levels of Mig6 expression could be expected to confer a growth advantage in the context of an EGFR-driven tumor, particularly in the face of high levels of EGFR expression resulting from increased *EGFR* copy number. Interestingly, *ERRFI1* deletions are highly correlated with coexisting EGFR amplification. Co-occurrence of mutations or copy number alterations in two genes in the same signaling pathway is atypical; such alterations are usually mutually exclusive, owing to the ability of a single lesion to activate the relevant oncogenic pathway. However, loss of one or both copies of *ERRFI1* could be expected to have little effect absent EGFR pathway activation because Mig6 requires phosphorylation by active EGFR to render it competent to inhibit and drive degradation of EGFR.

The lung cancer-associated EGFR mutants we studied here are clearly still sensitive to Mig6 inhibition biochemically and in cells, and the Mig6 Y394–Y395 site is phosphorylated in EGFR-mutant PC9 and HCC827 cells (Fig. 1c). These findings raise the question of how mutant or amplified EGFR escapes effective inhibition by Mig6. One possible mechanism is sub-stoichiometric expression of Mig6 relative to EGFR. Consistent with this, we find that over-expression of Mig6 blocks the ability of mutant EGFR to transform NIH-3T3 cells (Fig. 3). Structural differences in the mutant EGFR asymmetric dimer may also contribute to escape. Because the mutations promote the active conformation of the kinase, both subunits in the mutant dimer may contribute to EGFR signaling, whereas only the "receiver" subunit is active in ligand-stimulated WT EGFR. Thus, full inhibition of mutant EGFR may require a 2:2 stoichiometry of Mig6 to EGFR, as compared with a 1:2 stoichiometry in WT EGFR (Fig. 7b). In addition, the asymmetric dimer contact is likely to impede the access of Mig6 to the subunit in the activator position[18,49,50]. Although the isolated segment 2 interaction is of relatively low affinity, the structure we describe here may facilitate design of higher affinity cyclic peptide or peptidomimetic inhibitors that target the peptide-substrate binding site. Such an inhibitor, like Mig6 itself, could be expected to potently inhibit diverse oncogenic EGFR variants, including those that do not respond to available EGFR TKIs.

Online Methods

Quantitative Phosphoproteomic Analysis

Cells were lysed with 8 M urea supplemented with 1 mM activated Na_3VO_4. Proteins were reduced with 10 mM DTT at 50 °C for 1 hour and alkylated with 55 mM iodoacetamide at RT for 1 hour in the dark. Cell lysates were diluted to 1.6 M urea 100 mM $NH4HCO3$ and digested with trypsin at a 1:50 (enzyme:substrate) ratio. After incubation at 37 °C overnight, whole cell digests were acidified with 10% TFA to pH 3–4 and centrifuged to remove insoluble material. Peptides were desalted using a 96 well plate embedded with C18 resin (Waters, Milford, MA). Eluted peptides were freeze-dried and stored at −80 °C. Peptides were labeled with iTRAQ 4-plex reagents according to the manufacturer's protocol (114-WT

+EGF, 115-Ex20Ins, 116-Ex20Ins-KD, 117-CT DEL1). Briefly, iTRAQ reagent was reconstituted with 70 μL of ethanol, and peptides were resuspended with 30 μL of 0.5 M triethylammonium acetate bicarbonate. After mixing, the solution was incubated at room temperature for 1 hour. Then all four samples were combined and dried in a SpeedVac. To enrich tyrosine phosphorylated peptides, α-phosphotyrosine antibodies (20 μL of pTyr-100 from Cell Signaling Technology (Beverly, MA) and 20 μL of PT-66 from Sigma) were incubated with 16 μL of 50% protein G-agarose beads (Calbiochem) in 100 mM HEPES, 100 mM NaCl, pH 7.4 (IP buffer) at 4 °C for 8 hours on a rotator. After washing with IP buffer, 4 μL antibody-bead conjugate was added to iTRAQ-labeled peptides (solubilized in IP buffer) and the mixture was incubated at 4 °C overnight on a rotator. Beads were spun down at 4000 rpm and rinsed with 400 μL of IP buffer three times. Peptides were eluted with 40 μL of 15% acetonitrile/0.1% TFA for 15 min; the eluate was combined with 20 μL 80% acetonitrile/0.1% and loaded onto an Fe^{3+} activated self-packed IMAC column (360 μm O.D. χ 200 μm I.D. fused silica packed with 10 cm NTA silica from Qiagen)[51]. After washing with 80% acetonitrile/0.1% TFA and 0.01% acetic acid, phosphopeptides were directly eluted onto a C18 precolumn (100-μm I.D., 4 cm long; POROS 10R2) with 15 μL of 100 mM $(NH_4)_2HPO_4$, 1 mM EDTA. The precolumn was rinsed with 1% HOAc at 5 μL/min for 10 min and connected to a C18 analytical column (25-μm inner diameter, 10 cm long, 3-μm Monitor C18 resin). Peptides were eluted at a flow rate of ~5 nL/min with a 2 hours gradient: 1–25% B in 75 minutes, 25–40% B in 15 minutes, 40–70% B in 5 minutes, 70% B for 10 minutes, and 70–1% B in 5 minutes (A, 0.2 M HOAc; B, 70% MeCN, 0.2 M HOAc) using a NanoAcquity UPLC system with a precolumn split[52]. Eluted peptides were directly electrosprayed into a QStar-Elite (AB Sciex, Framingham, MA) mass spectrometer and subjected to MS/MS analysis with a data-dependent method. MS spectra were acquired in the range of 330 – 1500 amu for 1 second. A precursor was selected for MS/MS if its signal was over 40 counts and its charge state was 2+ to 5+. MS/MS spectra were acquired in the range of 108–1500 amu with fragment intensity multiplier of 6 and maximum accumulation time of 4 seconds. Up to five precursors could be selected for each cycle and then were excluded for 30 s after MS/MS spectra were acquired. Data were converted to Mascot Generic Format (mgf) with ABSciex MS Data converter version 1.3 and searched against a human refseq database using Mascot 2.2 with precursor and product ion tolerances of 0.5 Da. Search parameters specified fixed modifications of cysteine (carbamidomethylation) and peptide N-termini and lysine (4-plex iTRAQ) as well as variable modification of serine, threonine, tyrosine (phosphorylation) and methionine (oxidation). Multiplierz scripts[53] were used to filter results to a 1% FDR, remove hits with mass deviations >50 ppm, and extract iTRAQ reporter ion intensities. Ratios were corrected for source protein variations according to median values.

MALDI-MS and MS/MS Analysis of in vitro Kinase Reactions

Reactions were diluted with 0.1% TFA, and ~20 pmol peptide was desalted using micro C_{18} ZipTips® (Millipore, Billerica, MA). Peptides were deposited in a final volume of 1.5 μL directly onto a MALDI plate. Matrix (1 μL, 10 mg/mL alpha hydroxyl cinnamic acid in 70% acetonitrile with 0.1% TFA and 120 μg/mL diammonium citrate) was added to each sample spot and allowed to air dry. Samples were analyzed using a 4800+ MALDI-TOF/TOF mass spectrometer (AB Sciex, Framingham, MA) in reflectron mode averaging 1500 laser shots

in a random, uniform pattern (30 sub-spectra, pass or fail, 50 shots/sub-spectrum) with a laser intensity of ~4000. MS/MS experiments were performed in reflectron mode averaging 5000 laser shots in a random uniform pattern (100 sub-spectra, pass or fail, 50 shots/sub-spectrum) with CID gas on and the precursor mass window set to relative with a value of 200 (FWHM). Relative amounts of pYY and YpY were determined from corresponding b5 ion signals in MALDI-MS/MS spectra. These signals were corrected for differences in ionization efficiency and b5 fragment ion production using a normalization factor derived in a separate MALDI-MS/MS analysis of an equimolar mixture of pYY and YpY peptides. Once the relative contribution of pYY and YpY toward the singly phosphorylated peptide signal in MS1 spectra were established, relative levels of all 4 peptides were calculated using additional normalization factors derived by performing MALDI-MS analysis of equimolar amounts of synthetic unphosphorylated and phosphorylated peptides. For reactions using Mig6 300-399, peptides were diluted with 100 mM ammonium bicarbonate (final concentration 100 ng/μL), reduced with DTT (10 mM) for 30 minutes at 56 °C, alkylated with 22.5 mM IAA for 30 minutes at room temperature in the dark, and digested with trypsin overnight at 37 °C. Peptides (~1.5 pmol) were analyzed by LC-MS/MS essentially as described[52]. Peptides were loaded via autosampler injection (NanoAcquity Sample Manager) onto a self-packed precolumn (4 cm POROS 10R2), resolved on an analytical column with integrated ESI emitter tip (spray voltage = 2.2 kV) using an HPLC gradient (0–35% B in 20 min; A=0.2 M acetic acid in water, B=0.2 M acetic acid in acetonitrile), and eluted into an Orbitrap XL mass spectrometer (Thermo Fisher Scientific). The mass spectrometer was programmed to subject the 8 most abundant precursors to MS/MS (linear ion trap detection, collision energy=35%) followed by targeted MS/MS scans for doubly charged ions of VSSTHYYLLPE, singly phosphorylated VSSTHYYLLPE, and doubly phosphorylated VSSTHYYLLPE. Dynamic exclusion was enabled with a repeat count of 1 and an exclusion time of 30 seconds. Signals were corrected for differences in peptide ionization efficiencies using normalization factors derived from LC-MS/MS analyses of synthetic peptides and phosphopeptides.

Expression Constructs

Wild-type *EGFR*, L747_E749del, A750P (Ex19Del), D770_N771insNPG (Ex20Ins), L858R/T790M, G719A, CTDel1 (deletion within 1010-1152 aa) mutant *EGFR* containing vectors were previously described[36,37,54]. cDNA fragment of wild-type Mig6 was generated by PCR reaction and resulting PCR amplicons were cloned into pCMV5-FLAG mammalian expression vector which expresses, respectively, M2-FLAG-tagged polypeptides. Y394F or Y394F Y395F or Y395F Mig6 mutants encoding plasmids were generated by QuikChange site-directed mutagenesis (Agilent) using pCMV5 Mig6 as templates. All plasmids were confirmed by sequencing.

Cell culture and Generation of Cell Lines

All NIH-3T3 cell lines stably expressing EGFR and/or Mig6 were established by retroviral infections and pooled as described previously[37]. NIH-3T3 and HEK-293T cells were purchased from ATCC and maintained in DMEM supplemented with either 10% bovine serum or 10% fetal bovine serum, respectively. PC9, HCC827 and A549 cells kindly provided by P. Janne (Dana-Farber Cancer Institute) were cultured in RPMI supplemented

with 10% fetal bovine serum. Transient transfection was performed using X-tremeGene 9 (Roche) according to manufacture's instruction. Epidermal growth factor (EGF, Biosource) stimulations were performed using 25 ng/ml for 5 minutes unless noted in the text. All cell lines above except NIH-3T3 cells were authenticated by DNA finger printing analysis (STR analysis).

Immunoblotting, Coimmunoprecipitation Analysis and Antibodies

Polyclonal pY394pY395 specific anti-Mig6 antibody was raised by immunizing with the peptide-SSTHpYpYLLPER (corresponding to Mig6 residues 390–400) and further affinity purified by Young In Frontier (Seoul, Republic of Korea). Antibodies against phospho-Erk1/2 (#4376S), phospho-Src (#2101S), phospho-Akt (#4058L), Myc tag (2276S), β-actin (#4967) and Mig6 (#2440) were purchased from Cell Signaling Technology. Anti-phospho-tyrosine (4G10, #05-321) as well as anti-vinculin (#V9131) and anti-FLAG (#F1804) antibodies were from Upstate Biotechnology and Sigma-Aldrich, respectively. Anti-HA (#923502) and anti-EGFR (#A300-388A) antibodies were from Covance and Bethyl Laboratories, respectively. Cells were lysed in RIPA buffer supplemented with protease inhibitors (Roche) and phosphatase inhibitors (Calbiochem) and subjected to immunoblotting. For immunoprecipitation, 200–500 μg of protein lysate were incubated with antibody and protein A agarose for 3 to 12 hours at 4 °C.

Original images of gels and blots used in this study can be found in Supplementary Data Set 1.

Anchorage-independent Growth Assay

Soft agar assays were conducted as previously described[50]. After 2–3 weeks, the colonies formed in soft agar were quantified by analysis of photographed images of soft agar using Image J software (NIH). The data were presented as a relative ratio in a graph following normalization to number of colonies formed by control cells (see figure legends). The data represent triplicate wells. Each assay was repeated a minimum of two times with comparable results.

shRNA Studies

Vectors with shRNA targeting c-Src and GFP were purchased from Sigma and viruses were produced using protocols from the RNAi Consortium (http://www.broadinstitute.org/rnai/trc). Target cells were plated the day prior to infection and subsequently incubated with diluted virus in 8 ug/mL polybrene for six hours. Virus infected cells were pooled and treated with puromycin for 1 week before conducting experiments.

Enzyme Kinetics

For in vitro enzyme kinetic and inhibition studies, wild type or mutant EGFR kinases (residues 696-1022 of the human EGFR) were expressed and purified as GST-fusion proteins in Sf9 insect cells essentially as described[55]. Kinetic parameters were determined using the ATP/NADH coupled assay system in a 96-well plate, as described previously [55]. The reaction mixture contained 0.5 mg/mL BSA, 2 mM MnCl$_2$, 1 mM PEP (2-(Phosphonooxy)-2-propenoic acid, Sigma-Aldrich, Cat. P-7002), 1 mM TCEP, 0.1 M

HEPES (pH7.5), 2.5 mM tyrosine kinase substrate poly[E$_4$Y] (P7244, Sigma-Aldrich), 1/50 of the final reaction mixture volume of PK/LDH enzyme (Pyruvate Kinase/Lactic Dehydrogenase enzymes from rabbit muscle, Cat. P-0294, Sigma-Aldrich), 0.5 mM NADH and 0.1~0.5 μM EGFR (0.1 μM for L858R, 0.5 μM for WT and 0.2 μM for T790M/V948R). 1 mM ATP was added last to start the reactions. Steady state initial velocity data were drawn from the slopes of the A$_{340}$ curves and fit to the Michaelis-Menten equation to determine V_m and K_m values. EGFR inhibition by Mig6 was measured using the same assay and K_i^{app} values were determined by fitting inhibition curves to the Morrison equation using Graphpad PRISM software.

Semisynthetic Mig6 Phosphoproteins

GST-Mig6 (330-389) was cloned into pTXB1 vector (New England Biolab) and transformed into E. coli BL21 (DE3). Transformed cells were cultured at 37 °C until A$_{600}$ reached 0.8, and then induced with 500 μM IPTG to overexpress the GST- Mig6 (330–389) - intein-CBD fusion protein. Cell pellets were resuspended in 1X PBS with 5% Glycerol and 1 mM TCEP, 1 tablet of protease inhibitor cocktail (Roche) and lysed by sonication. After centrifugation at 17,000 rpm for 40 min to remove cell debris, the supernatant was collected, incubated with GST sepharose (GE healthcare) beads for affinity purification and then eluted with 10 mM glutathione. Eluted protein was treated with TEV protease for 6h to remove the GST fusion partner and then loaded onto chitin beads (New England Biolabs) for affinity purification and ligation with peptide. The chitin bead-bound fusion protein was washed with washing buffer (500 mM NaCl 50 mM HEPES pH 7.4, 1 mM TCEP), and then equilibrated in cleavage buffer (50 mM HEPES pH 7.4, 150 mM NaCl, 0.1 mM TCEP). Addition of 200 mM 2-mercaptoethane sulfonate (MESNA, Sigma-Aldrich) in cleavage buffer at 4°C for 12 hours induced release of the Mig6-thioester. To obtain the desired semisynthetic phosphoproteins, 1 mM of synthetic Mig6 phosphopeptide (CSTHpYYLLPE, CSTHYpYLLPE, or CSTHpYpYLLPE) was added to the cleaved Mig6 thioester solution. The ligation reaction was allowed to proceed for 48 hours at 4 °C. The ligated phospho-Mig6 proteins were purified with cation exchange chromatography (Mono S) and size-exclusion chromatography (Superdex 75). The unphosphorylated Mig6 (330-399) was obtained by E.coli expression and purified using the same conditions employed for the semisynthetic Mig6 phosphoproteins. The correct masses and phosphorylation state of each of the Mig6 proteins was verified by mass spectrometry.

Structure Determination

The L858R mutant EGFR kinase domain was crystallized as previously described[55]. Synthetic phosphopeptides based on the Mig6 Y394 and Y395 phosphorylation sites (with sequences SSTHYpYLLPE and SSTHpYpYLLPE) were soaked into the apo-crystals in reservoir solution supplemented with 1 mM peptide for 5 hours. For co-crystallization of WT EGFR with segment 1+2 phospho-Mig6 (330-399), the protein complex was prepared by size-exclusion chromatography using by (Superdex 200, GE healthecare) and concentrated to 2.5mg/ml. Crystals were obtained by hanging drop vapor diffusion against 25% polyethylene glycol 3350, 200 mM Ammonium acetate and 100 mM Bis-Tris (pH5.5). All diffraction data were collected using a wavelength of 0.979 Å on the NE-CAT beamlines ID24-C and E, Argonne National Laboratory, at 100K and were processed and merged with

HKL2000 (ref. 56). The peptide complex structures were determined by molecular replacement using the EGFR L858R kinase structure as a search model (PDB entry 2ITV). L858R-mutant EGFR was used in this study, but the mutation does not appear to affect interactions with Mig6. The Mig6 segment 1+2 complex structure was determined by molecular replacement using the structure of EGFR in complex with Mig6 segment 1 as a search model (PDB entry 2RF9). This structure contains two closely similar EGFR–Mig6 complexes in the crystallographic asymmetric unit (r.m.s.d. 0.39); molecule "A" is described and illustrated here. For all structures, the Mig6 sequences were modeled into closely fitting positive Fo-Fc density and repeated rounds of manual refitting and crystallographic refinement were performed using COOT[57] and PHENIX[58]. Crystallographic data collection and refinement statistics are presented in Table 1.

Size Exclusion Chromatography with EGFR-Mig6 Complex

The EGFR L858R kinase (residues 696-1022) was combined with a two-fold molar excess of unphosphorylated Mig6 (residues 330-399) and incubated at room temperature with 1 mM ATP in reaction buffer buffer (0.1M HEPES, pH7.5, 0.1M NaCl, 2mM TCEP, 2mM $MnCl_2$). After 20 minutes incubation, 20 mM EDTA was added to quench the reaction and the reaction mixture was subjected to size-exclusion chromatography (Superose 200). Eluted fractions were analyzed by SDS-PAGE and Western blotting with anti-pMig6 (pY394pY395).

Off-rate determination

A two-fold molar excess of EGFR L858R kinase (residues 696-1022) was combined with unphosphorylated GST-Mig6 (residues 330-399) in reaction buffer (0.1M HEPES, pH7.5, 0.1M NaCl, 2mM TCEP, 2mM $MnCl_2$) with or without 10 mM ATP. After 20 minutes incubation at room temperature, identical aliquots of the reaction mixture were loaded onto GST sepharose beads in spin columns and vigorously washed with reaction buffer. Beads in each spin column were maintained under flow with reaction buffer for the indicated time periods and then eluted with 10 mM glutathione in reaction buffer. Eluted samples were analyzed by SDS-PAGE, and the molar ratio of EGFR and Mig6 proteins was quantified by densitometry (ImageQuant, GE healthcare).

Genomic Analyses

Copy-number data from TCGA (refs. 21,59) were analyzed as described[46] to identify recurrent alterations and correlated and anticorrelated events. Genome-wide results of the recurrence analyses are available at www.broadinstitute.org/tcga under the "2014-07-08 stddata_2014_06_14" analysis version. Clustering of copy number profiles was performed using Ward's method as implemented in R and a Euclidean distance metric on a matrix of 10 kb bins across chromosome 1p. Samples were called as having *EGFR* focal amplifications or *ERRFI1* focal deletions if they exhibited focal copy-number alterations surpassing 0.1 and −0.1 copies in amplitude, respectively. Mutation calls for *FUBP1* were taken from TCGA analyses[21,59].

Author Manuscript

Supplementary Material

Refer to Web version on PubMed Central for supplementary material.

Acknowledgments

References

1. Fiorentino L, et al. Inhibition of ErbB-2 mitogenic and transforming activity by RALT, a mitogen-induced signal transducer which binds to the ErbB-2 kinase domain. Mol Cell Biol. 2000; 20:7735–50. [PubMed: 11003669]

2. Hackel PO, Gishizky M, Ullrich A. Mig-6 is a negative regulator of the epidermal growth factor receptor signal. Biol Chem. 2001; 382:1649–62. [PubMed: 11843178]

3. Xu D, Makkinje A, Kyriakis JM. Gene 33 is an endogenous inhibitor of epidermal growth factor (EGF) receptor signaling and mediates dexamethasone-induced suppression of EGF function. J Biol Chem. 2005; 280:2924–33. [PubMed: 15556944]

4. Segatto O, Anastasi S, Alema S. Regulation of epidermal growth factor receptor signalling by inducible feedback inhibitors. J Cell Sci. 2011; 124:1785–93. [PubMed: 21576352]

5. Fiorini M, et al. Expression of RALT, a feedback inhibitor of ErbB receptors, is subjected to an integrated transcriptional and post-translational control. Oncogene. 2002; 21:6530–9. [PubMed: 12226756]

6. Zhang YW, Vande Woude GF. Mig-6, signal transduction, stress response and cancer. Cell Cycle. 2007; 6:507–13. [PubMed: 17351343]

7. Anastasi S, Baietti MF, Frosi Y, Alema S, Segatto O. The evolutionarily conserved EBR module of RALT/MIG6 mediates suppression of the EGFR catalytic activity. Oncogene. 2007; 26:7833–46. [PubMed: 17599051]

8. Zhang X, et al. Inhibition of the EGF receptor by binding of MIG6 to an activating kinase domain interface. Nature. 2007; 450:741–4. [PubMed: 18046415]

9. Descot A, et al. Negative regulation of the EGFR-MAPK cascade by actin-MAL-mediated Mig6/Errfi-1 induction. Mol Cell. 2009; 35:291–304. [PubMed: 19683494]

10. Frosi Y, et al. A two-tiered mechanism of EGFR inhibition by RALT/MIG6 via kinase suppression and receptor degradation. J Cell Biol. 2010; 189:557–71. [PubMed: 20421427]

11. Ying H, et al. Mig-6 controls EGFR trafficking and suppresses gliomagenesis. Proc Natl Acad Sci U S A. 2010; 107:6912–7. [PubMed: 20351267]

12. Ferby I, et al. Mig6 is a negative regulator of EGF receptor-mediated skin morphogenesis and tumor formation. Nat Med. 2006; 12:568–73. [PubMed: 16648858]

13. Zhang YW, et al. Evidence that MIG-6 is a tumor-suppressor gene. Oncogene. 2007; 26:269–76. [PubMed: 16819504]

14. Maity TK, et al. Loss of MIG6 Accelerates Initiation and Progression of Mutant Epidermal Growth Factor Receptor-Driven Lung Adenocarcinoma. Cancer Discov. 2015

15. Anastasi S, et al. Loss of RALT/MIG-6 expression in ERBB2-amplified breast carcinomas enhances ErbB-2 oncogenic potency and favors resistance to Herceptin. Oncogene. 2005; 24:4540–8. [PubMed: 15856022]

16. Makkinje A, et al. Gene 33/Mig-6, a transcriptionally inducible adapter protein that binds GTP-Cdc42 and activates SAPK/JNK. A potential marker transcript for chronic pathologic conditions,

such as diabetic nephropathy. Possible role in the response to persistent stress. J Biol Chem. 2000; 275:17838–47. [PubMed: 10749885]

17. Anastasi S, et al. Feedback inhibition by RALT controls signal output by the ErbB network. Oncogene. 2003; 22:4221–34. [PubMed: 12833145]

18. Wang Z, et al. Mechanistic insights into the activation of oncogenic forms of EGF receptor. Nat Struct Mol Biol. 2011; 18:1388–93. [PubMed: 22101934]

19. Lemmon MA, Schlessinger J. Cell signaling by receptor tyrosine kinases. Cell. 2010; 141:1117–34. [PubMed: 20602996]

20. Kandoth C, et al. Mutational landscape and significance across 12 major cancer types. Nature. 2013; 502:333–9. [PubMed: 24132290]

21. Brennan CW, et al. The somatic genomic landscape of glioblastoma. Cell. 2013; 155:462–77. [PubMed: 24120142]

22. Cancer Genome Atlas Research, N. Comprehensive molecular profiling of lung adenocarcinoma. Nature. 2014; 511:543–50. [PubMed: 25079552]

23. Sharma SV, Bell DW, Settleman J, Haber DA. Epidermal growth factor receptor mutations in lung cancer. Nat Rev Cancer. 2007; 7:169–81. [PubMed: 17318210]

24. Mok TS, et al. Gefitinib or carboplatin-paclitaxel in pulmonary adenocarcinoma. N Engl J Med. 2009; 361:947–57. [PubMed: 19692680]

25. Yu HA, Pao W. Targeted therapies: Afatinib--new therapy option for EGFR-mutant lung cancer. Nat Rev Clin Oncol. 2013; 10:551–2. [PubMed: 23959269]

26. Chong CR, Janne PA. The quest to overcome resistance to EGFR-targeted therapies in cancer. Nat Med. 2013; 19:1389–400. [PubMed: 24202392]

27. Lee JC, et al. Epidermal growth factor receptor activation in glioblastoma through novel missense mutations in the extracellular domain. PLoS Med. 2006; 3:e485. [PubMed: 17177598]

28. Francis JM, et al. EGFR variant heterogeneity in glioblastoma resolved through single-nucleus sequencing. Cancer Discov. 2014; 4:956–71. [PubMed: 24893890]

29. Wong AJ, et al. Structural alterations of the epidermal growth factor receptor gene in human gliomas. Proc Natl Acad Sci U S A. 1992; 89:2965–9. [PubMed: 1557402]

30. Verhaak RG, et al. Integrated genomic analysis identifies clinically relevant subtypes of glioblastoma characterized by abnormalities in PDGFRA, IDH1, EGFR, and NF1. Cancer Cell. 2010; 17:98–110. [PubMed: 20129251]

31. Guha U, et al. Comparisons of tyrosine phosphorylated proteins in cells expressing lung cancer-specific alleles of EGFR and KRAS. Proc Natl Acad Sci U S A. 2008; 105:14112–7. [PubMed: 18776048]

32. Wolf-Yadlin A, et al. Effects of HER2 overexpression on cell signaling networks governing proliferation and migration. Mol Syst Biol. 2006; 2:54. [PubMed: 17016520]

33. Wang Z, et al. Tyrosine phosphorylation of mig6 reduces its inhibition of the epidermal growth factor receptor. ACS Chem Biol. 2013; 8:2372–6. [PubMed: 24004111]

34. Ficarro SB, et al. Magnetic bead processor for rapid evaluation and optimization of parameters for phosphopeptide enrichment. Anal Chem. 2009; 81:4566–75. [PubMed: 19408940]

35. Guo A, et al. Signaling networks assembled by oncogenic EGFR and c-Met. Proc Natl Acad Sci U S A. 2008; 105:692–7. [PubMed: 18180459]

36. Cho J, et al. Glioblastoma-derived epidermal growth factor receptor carboxyl-terminal deletion mutants are transforming and are sensitive to EGFR-directed therapies. Cancer Res. 2011; 71:7587–96. [PubMed: 22001862]

37. Greulich H, et al. Oncogenic transformation by inhibitor-sensitive and -resistant EGFR mutants. PLoS Med. 2005; 2:e313. [PubMed: 16187797]

38. Yasuda H, et al. Structural, biochemical, and clinical characterization of epidermal growth factor receptor (EGFR) exon 20 insertion mutations in lung cancer. Sci Transl Med. 2013; 5:216ra177.

39. Galisteo ML, Yang Y, Urena J, Schlessinger J. Activation of the nonreceptor protein tyrosine kinase Ack by multiple extracellular stimuli. Proc Natl Acad Sci U S A. 2006; 103:9796–801. [PubMed: 16777958]

40. Shen F, Lin Q, Gu Y, Childress C, Yang W. Activated Cdc42-associated kinase 1 is a component of EGF receptor signaling complex and regulates EGF receptor degradation. Mol Biol Cell. 2007; 18:732–42. [PubMed: 17182860]

41. Muir TW, Sondhi D, Cole PA. Expressed protein ligation: a general method for protein engineering. Proc Natl Acad Sci U S A. 1998; 95:6705–10. [PubMed: 9618476]

42. Silverman RB. Mechanism-based enzyme inactivators. Methods Enzymol. 1995; 249:240–83. [PubMed: 7791614]

43. Carpentier JL, White MF, Orci L, Kahn RC. Direct visualization of the phosphorylated epidermal growth factor receptor during its internalization in A-431 cells. J Cell Biol. 1987; 105:2751–62. [PubMed: 2447100]

44. Bose R, Holbert MA, Pickin KA, Cole PA. Protein tyrosine kinase-substrate interactions. Curr Opin Struct Biol. 2006; 16:668–75. [PubMed: 17085043]

45. Bettegowda C, et al. Mutations in CIC and FUBP1 contribute to human oligodendroglioma. Science. 2011; 333:1453–5. [PubMed: 21817013]

46. Zack TI, et al. Pan-cancer patterns of somatic copy number alteration. Nat Genet. 2013; 45:1134–1140. [PubMed: 24071852]

47. Hopkins S, et al. Mig6 is a sensor of EGF receptor inactivation that directly activates c-Abl to induce apoptosis during epithelial homeostasis. Dev Cell. 2012; 23:547–59. [PubMed: 22975324]

48. Bagchi A, Mills AA. The quest for the 1p36 tumor suppressor. Cancer Res. 2008; 68:2551–6. [PubMed: 18413720]

49. Red Brewer M, et al. Mechanism for activation of mutated epidermal growth factor receptors in lung cancer. Proc Natl Acad Sci U S A. 2013; 110:E3595–604. [PubMed: 24019492]

50. Cho J, et al. Cetuximab response of lung cancer-derived EGF receptor mutants is associated with asymmetric dimerization. Cancer Res. 2013; 73:6770–9. [PubMed: 24063894]

References for Online Methods

51. Adelmant, G., et al. Affinity and chemical enrichment for mass spectrometry-based proteomics analyses. In: Ivanov, A.; L.A., editors. Sample preparation in biological mass spectrometry. Springer, Dordrecht; The Netherlands: 2011. p. 437-486.

52. Ficarro SB, et al. Improved electrospray ionization efficiency compensates for diminished chromatographic resolution and enables proteomics analysis of tyrosine signaling in embryonic stem cells. Anal Chem. 2009; 81:3440–7. [PubMed: 19331382]

53. Parikh J, et al. multiplierz: an extensible API based desktop environment for proteomics data analysis. BMC Bioinformatics. 2009; 10:364. [PubMed: 19874609]

54. Yuza Y, et al. Allele-dependent variation in the relative cellular potency of distinct EGFR inhibitors. Cancer Biol Ther. 2007; 6:661–7. [PubMed: 17495523]

55. Yun CH, et al. Structures of lung cancer-derived EGFR mutants and inhibitor complexes: mechanism of activation and insights into differential inhibitor sensitivity. Cancer Cell. 2007; 11:217–27. [PubMed: 17349580]

56. Otwinowski Z, Borek D, Majewski W, Minor W. Multiparametric scaling of diffraction intensities. Acta Crystallogr A. 2003; 59:228–34. [PubMed: 12714773]

57. Emsley P, Lohkamp B, Scott WG, Cowtan K. Features and development of Coot. Acta Crystallogr D Biol Crystallogr. 2010; 66:486–501. [PubMed: 20383002]

58. Adams PD, et al. PHENIX: a comprehensive Python-based system for macromolecular structure solution. Acta Crystallogr D Biol Crystallogr. 2010; 66:213–21. [PubMed: 20124702]

59. Cancer Genome Atlas Research, N. et al. Comprehensive, Integrative Genomic Analysis of Diffuse Lower-Grade Gliomas. N Engl J Med. 2015; 372:2481–98. [PubMed: 26061751]
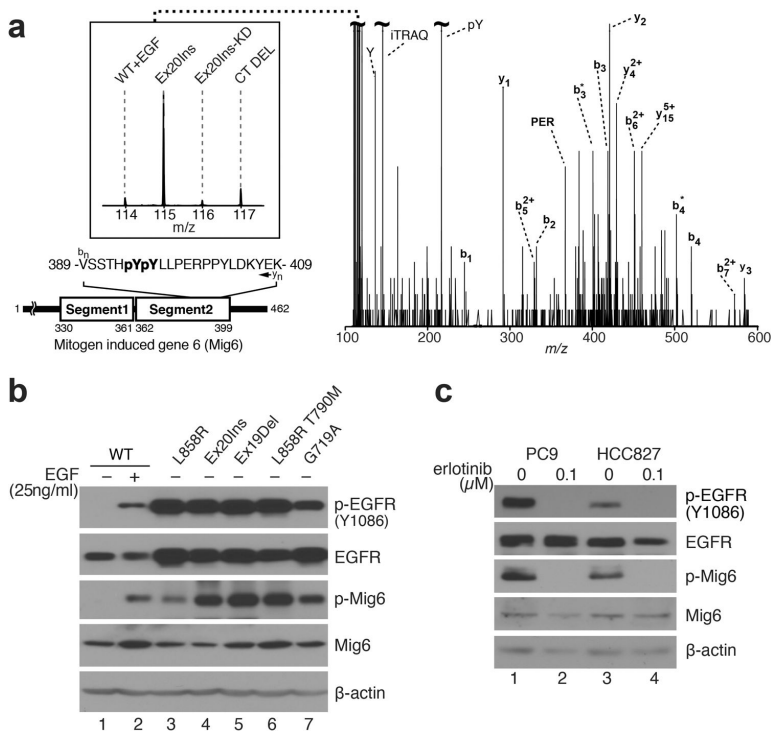
Figure 1. Identification and validation of EGFR-driven phosphorylation of Mig6 on Y394–Y395
a, Tandem mass spectrum identifying the iTRAQ-labeled pY394–pY395 Mig6 peptide in NIH-3T3 cells stably expressing WT EGFR or indicated mutants. Relevant y-type (C-terminal) and b-type (N-terminal) fragment ions are labeled, as are the immonium ions corresponding to tyrosine (Y), phosphotyrosine (pY), the intact iTRAQ moiety (iTRAQ), and an internal fragment ion consisting of the amino acids Pro-Glu-Arg (PER). The iTRAQ reporter ions corresponding to Mig6 derived from WT EGFR (with EGF stimulation), Ex20Ins, Ex20Ins/D837A (KD) or C-terminal domain deletion EGFR mutant (CTDel1, which deletes residues 1010-1152) are shown in the inset, along with the peptide sequence and location of the tyrosine phosphorylation sites (pYpY). **b**, Western blots probing Mig6 Y394–Y395 phosphorylation in NIH-3T3 cells stably expressing WT or mutant EGFR. Cell lysates were subjected to SDS-PAGE followed by immunoblotting with antibodies against EGFR, p-EGFR, Mig6 and p-Mig6 (pY394pY395). **c**, Western blots probing Mig6 Y394–Y395 phosphorylation in EGFR-mutant lung cancer cell lines. Cell lysates prepared from PC9 or HCC827 cell lines were immunoblotted with the same antibodies used in (**b**), either untreated or following erlotinib treatment (0.1 μM) for 3 hours.
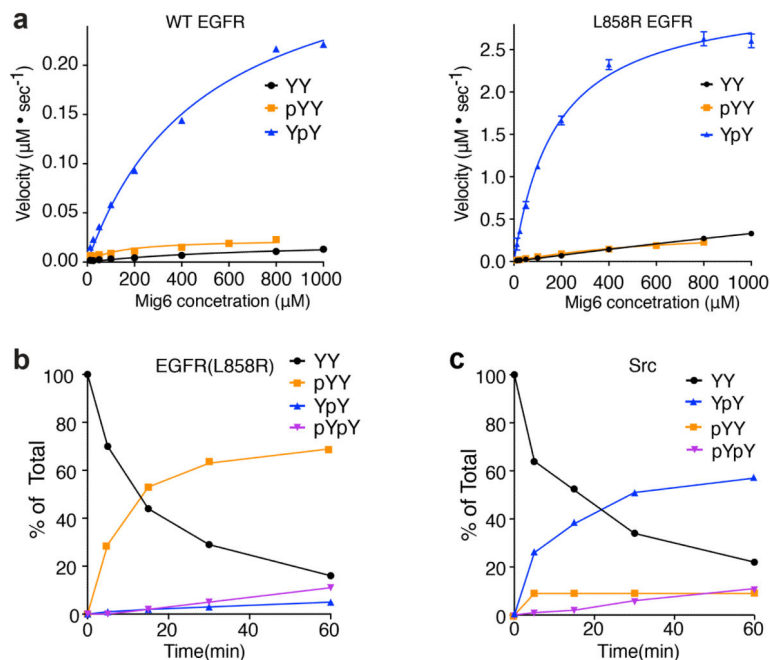
Figure 2. Characterization of Mig6 Y394–Y395 peptides as substrates for EGFR and Src

a, EGFR kinases assays using synthetic peptides corresponding to residues 390-399 of Mig6 as substrates for WT EGFR (left panel) or the L858R mutant (right panel). Steady-state reaction velocities were measured at a range of concentrations for Mig6 peptides that were unphosphorylated (YY), phosphorylated on Y394 (pYY), or phosphorylated on Y395 (YpY). Values are the average of three replicates and are plotted ±SEM. **b** and **c**, Mass spectrometry-based analysis of the products of phosphorylation of Mig6 390-399 by L858R-mutant EGFR (**b**) or Src (**c**). Unphosphorylated Mig6 peptide (YY) was used as a substrate and the products of the reaction and remaining substrate were quantitated as a function of time using mass spectrometry.
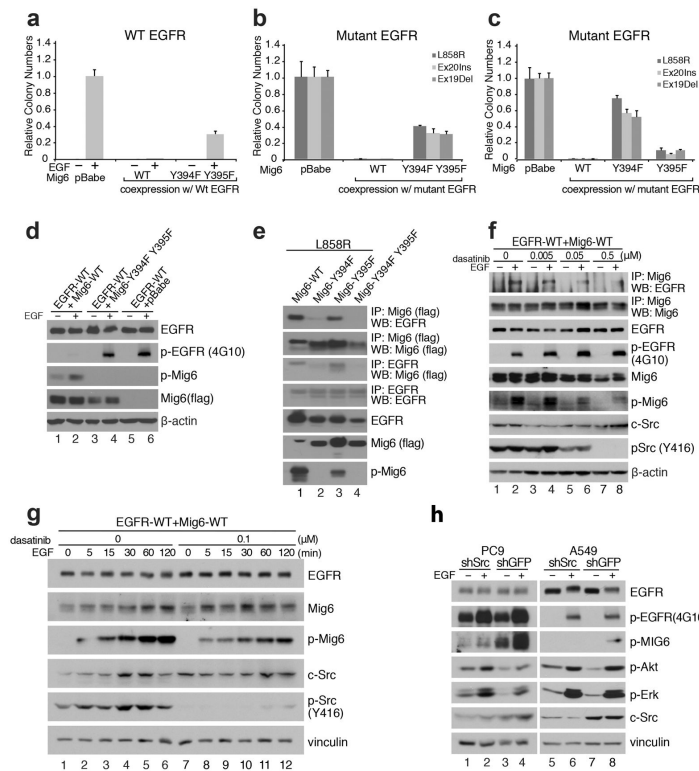
Figure 3. Phosphorylation of Mig6 on Y394-Y395 is essential for binding and inhibition of EGFR and is modulated by Src

a–c, Colony formation assays in soft agar with NIH-3T3 cells stably coexpressing WT or mutant EGFR together with flag-tagged WT or mutant Mig6 (Y394F, Y395F or Y394F Y395F). The bar graph depicts the relative number of colonies formed in each experimental condition normalized to the vector control (pBabe, n=3, mean +SD). **d**, Western blots probing EGFR and Mig6 phosphorylation in NIH-3T3 cells expressing EGFR alone or with WT or mutant Mig6, as indicated. **e**, Coimmunoprecipitation and immunoblotting analysis of cell lysates prepared from 293T cells coexpressing L858R EGFR and Mig6 variants with antibodies against flag-tagged Mig6 or EGFR. **f**, Western blots showing the effect of dasatinib on the phosphorylation and coimmunoprecipitation of EGFR and Mig6 in NIH-3T3 cells. Cells stably coexpressing WT Mig6 and WT EGFR were treated with indicated concentrations of dasatinib, and the resulting cell lysates were used for coimmunoprecipitation analysis and western blotting. **g**, Immunoblots showing the effect of dasatinib on EGF-stimulated phosphorylation of Mig6 and Src in NIH-3T3 cells stably expressing WT EGFR and WT Mig6. Cells were pretreated with dasatinib or left untreated prior to EGF-stimulation and lysates were subjected to immunoblotting analysis with antibodies as indicated. **h**, Western blots probing phosphorylation of EGFR, Mig6, Akt and Erk in cell lysates prepared from PC9 or A549 cells stably expressing shRNA targeting either c-Src or GFP (control) before or after EGF treatment.
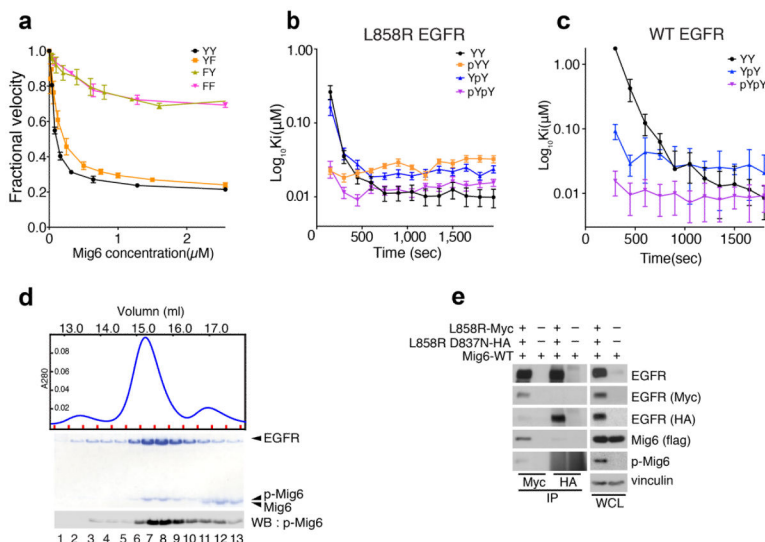
Figure 4. Phosphorylation of Y394 increases the potency of Mig6 by two orders of magnitude and is the basis for activity-based inhibition of EGFR

a, Kinase assays measuring inhibition of L858R EGFR by Mig6 segment 1+2 (residues 330–399). The kinase was preincubated with increasing concentrations of WT Mig6 or Mig6 bearing the indicated tyrosine to phenylalanine mutations and reaction velocity was measured at steady state. **b** and **c**, Time-resolved kinase assays with Mig6 phosphorylation variants. K_i values were determined at 150 second intervals for inhibition of L858R (**b**) and WT (**c**) EGFR kinases by semi-synthetic Mig6 proteins phosphorylated on Y394 and Y395 as indicated. In a–c, values are the average of three replicates and are plotted ±SEM. **d**, Size-exclusion chromatography analysis of Mig6–EGFR product complex. An excess of unphosphorylated Mig6 segment 1+2 (residues 330-399) was incubated with EGFR under reaction conditions and the mixture was then analyzed by size-exclusion chromatography followed by SDS-PAGE and western blotting for phospho-Mig6. The elution profile is shown in the upper panel, aligned with Coomassie-stained SDS-PAGE of corresponding elution fractions (middle panel). Free Mig6 is predominately unphosphorylated, while EGFR-bound Mig6 (co-eluting with EGFR at ~15 ml) is phosphorylated, as assessed by the shift in electrophoretic mobility (see Supplemental Fig. S4b) and western blotting with the Mig6-pY394pY395 specific antisera (lower panel). **e**, Co-immunoprecipitation experiment comparing binding of Mig6 to active versus kinase-dead L858R EGFR. Lysates prepared from HEK-293T cells transiently cotransfected with expression constructs of Myc-tagged L858R and HA-tagged L858R D837N (kinase dead) EGFR along with WT Mig6 were subjected to coimmunoprecipitation and immunoblotting as indicated.
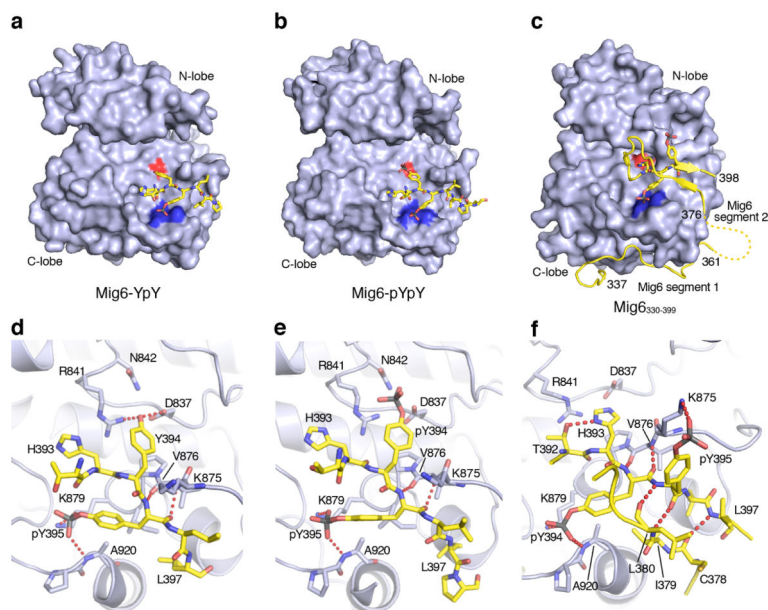
Figure 5. Structural snapshots of Mig6 inhibition of EGFR

a–c, Overall views of crystal structures of the EGFR kinase domain bound to phosphorylated Mig6 constructs. The EGFR kinase is shown in a surface representation with Asp 837, the catalytic base, colored red to indicate the phospho-acceptor pocket and the surface of Lys879 and Ala920 shaded dark blue to indicate the priming recognition pocket. **a**, Mig6-pYpY peptide, residues 390-399, bound to EGFR. **b**, Mig6-pYpY peptide, residues 390-399, bound to EGFR. **c**, Structure of doubly-phosphorylated Mig6 segment 1 + 2 bound to EGFR. Mig6 residues 337–361 (segment 1) and 376–398 (segment 2) are included in the model. The intervening 14 residues are unstructured. The kinase exhibits inactive features in this structure; the "DFG" motif is flipped and the C-helix is displaced into an outward, inactive position. These deviations from the stereotypical active conformation appear unrelated to binding of Mig6, and we expect that Mig6 could bind in a similar manner to the fully active conformation of the kinase. **d–f**, Detailed views of Mig6-EGFR interactions for the structures shown in panels a–c above. Hydrogen bonds are indicated by dashed red lines. In **f**, note that Mig6 residues 378–380 form a short β-strand that hydrogen bonds with residues 395–397 of Mig6. See also Supplementary Fig. S7.
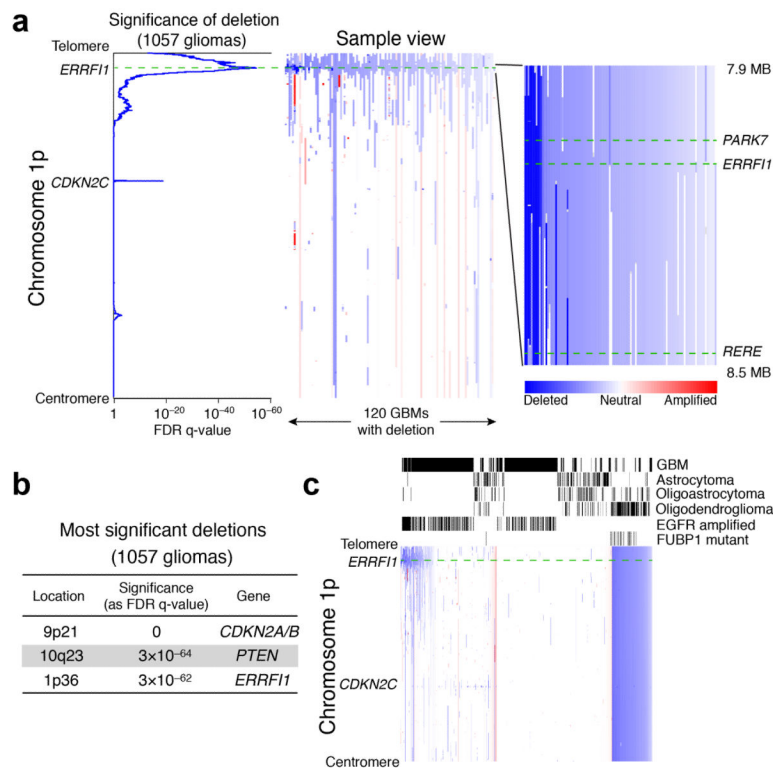
Figure 6. Analysis of chromosome 1p copy number alterations across 1057 gliomas
a, Significance of chromosome 1p deletions in 1057 gliomas (false discovery rate q-value, left panel); heatmaps of copy numbers in 120 glioblastomas across 1p (center panel) and in a 600 kb window around *ERRFI1* (right panel). *ERRFI1*, *CDKN2C*, *PARK7*, and *RERE* indicate the locations of these genes. **b**, The three most significantly recurrent deletions across 1057 gliomas. **c**, Unsupervised clustering of 1p copy number profiles (shown as heatmaps, bottom) among 1057 gliomas. Gliomas with focal *ERRFI1* deletions clustered to the left; those with loss of all of 1p clustered to the right. The histology and *EGFR* and *FUBP1* status of these gliomas is indicated above the heatmap.
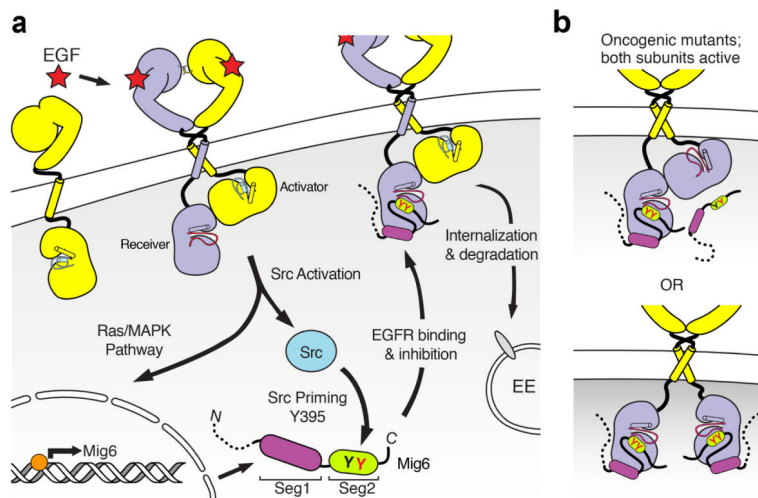
Figure 7.
Model for mechanism of feedback inhibition of EGFR by Mig6. **a**, EGFR signaling induces expression of Mig6 via the Ras Map kinase pathway. EGFR also activates Src, which primes Mig6 by phosphorylating Y395. Mig6 binds EGFR and is phosphorylated on Y394, which renders it a potent inhibitor of EGFR. After phosphorylation, Mig6 remains bound to EGFR and segment 2 rearranges to block the peptide-substrate binding cleft. A single Mig6 molecule should be sufficient to inactivate the WT receptor, as only one subunit in the asymmetric dimer is active and able to phosphorylate Mig6. **b**, By contrast, the mutationally activated receptor may require a 2:2 stoichiometry of Mig6 for inactivation, as both subunits are expected to be active. Inhibition of the subunit in the "activator" position could be impaired, because the segment 1 binding site is blocked by the asymmetric dimer interaction (upper panel).

Table 1

Data collection and refinement statistics.

	L858R EGFR+Mig6 YpY (residues 390-399)	L858R EGFR+Mig6 pYpY (residues 390-399)	WT EGFR+Mig6 segment 1+2 (residues 330-399, pYpY)
Data collection			
Space group	I23	I23	P2
Cell dimensions			
a, b, c (Å)	143.8, 143.8, 143.8	144.689, 144.6, 144.6	58.459, 81.865, 96.19
α, β, γ (°)	90.0, 90.0, 90.0	90.0, 90.0, 90.0	90.0, 106.67, 90.0
Resolution (Å)	$102.3 - 2.90\ (2.95)^a$	102.3 – 3.25 (3.32)	50–2.70(2.75)
R_{merge}	0.115 (0.149)	0.123 (0.561)	0.112(0.601)
$I/\sigma I$	6.4 (1.9)	10.3 (1.5)	9.1 (1.5)
Completeness (%)	99.2 (100)	87.7 (92.6)	96.5(87.3)
Redundancy	3.6 (3.6)	4.1 (4.0)	2.8(2.4)
Refinement			
Resolution (Å)	45.482–2.90	45.755–3.25	45.9–2.70
No. Reflections	11,009	7,110	20,535
R_{work}/ R_{free}	0.211/0.239	0.2005/0.2533	0.178/0.231
No. Atoms			
Protein	2517	2512	5178
Water	54	49	96
B-factors			
Protein	78.80	69.94	45.30
Water	79.70	66.70	37.00
R.m.s deviations			
Bond lengths (Å)	0.004	0.005	0.009
Bond angles (°)	0.907	0.947	1.20

[a] Values in parentheses are for highest-resolution shell.